Contribution of modeling to explain the depassivation of chromia-forming alloys in molten glasses

V. Szczepan, Carine Petitjean, P.J. Panteix, M. Vilasi

Version of Record: https://www.sciencedirect.com/science/article/pii/S0010938X21004637
Manuscript_e9abb01a7b8a65258b948c945f7e9707

Contribution of modeling to explain the depassivation of chromia-forming alloys in molten glasses

V. Szczepan[1], C. Petitjean[1], P.J. Panteix[1], M. Vilasi[1]

[1]Université de Lorraine, CNRS, IJL, F-54011 Nancy, France

Abstract

The corrosion of chromia-forming alloys by molten glass is an issue encountered in industrial processes such as glass fiber production or nuclear waste vitrification. A model of the corrosion of such alloys in molten glass media is developed in this work. This simple model predicts the corrosion state of the alloy (passive of active) and the evolution of the Cr_2O_3 layer thickness with a low number of input parameters. Furthermore, the model allows to explain the depassivation of the alloy by identifying the conditions involving a lack of oxygen supply in the liquid towards the oxide.

Keyword

Modeling, Corrosion, Glass, Chromia-forming alloys

1. Introduction

Chromia-forming alloys are commonly encountered in glass industry for the production of glass fiber or in nuclear applications as vitrification processes of nuclear wastes [1,2]. Such alloys are able to form a compact chromia (Cr_2O_3) layer by high temperature oxidation [3–6]. This oxide layer protects the alloy from a fast-active corrosion induced by a direct contact between the alloy and the molten glass: the alloy is thus passivated by chromia. The low solubility of chromia in molten silicates [2,7–10] ensures the durability of this intrinsic protection. For instance, Abdullah *et al*. [11] showed that chromia-forming alloys are far more efficient to withstand molten glass corrosion than alumina-forming alloys [7]. In certain conditions, a depassivation occurs, corresponding to the loss of the protective oxide layer (from passive state to active state). This phenomenon has been previously observed on chromia-forming alloys (e.g. Ni-30(wt.%)Cr and pure Cr) immersed in simplified molten silicates, and the influence of melt composition and temperature has been emphasized [12]. Recently, the concept of competition between simultaneous formation and dissolution of the oxide has been introduced to explain the different behaviours of chromia-forming alloys confronted to corrosion by molten silicates with various compositions [2,12]. Some authors [12–14] showed that in some cases, the chromia layer keeps growing when it is immersed in a molten glass, meaning that the formation of chromia due to the oxidation of the alloy is overcoming its dissolution by chemical reaction and diffusion in the liquid [2,9].

Based on the idea of an oxide layer simultaneously submitted to a parabolic formation by oxidation [15–17] and to a parabolic dissolution rate, Gheno *et al*. [18–20] proposed the following expression to describe the evolution of the oxide thickness.

$$\frac{de}{dt} = \frac{k_p}{e} - \sqrt{\frac{k_d}{2t}} \qquad \text{eq. 1}$$

With e the oxide thickness (m), k_p the parabolic oxidation constant of the oxide ($m^2\ s^{-1}$), k_d the parabolic dissolution constant of the oxide ($m^2\ s^{-1}$) and t the time (s). It is possible to show that this equation is always rendering a parabolic growth of the oxide. If the initial oxide thickness is superior to 0, the oxide thickness decreases first and then tends to a parabolic growth as shown by Gheno *et al*. [18–20]. The expression of the global parabolic growth of the oxide g ($m^2\ s^{-1}$) is given by the following equation.

$$e = \sqrt{2g} \cdot \sqrt{t} = \left(\sqrt{\frac{k_d}{2} + 2k_p} - \sqrt{\frac{k_d}{2}} \right) \cdot \sqrt{t} \qquad \text{eq. 2}$$

Schmucker *et al.* [14,21] used the equation 1 and parameters determined independently through experimental measurements [2,5] to simulate the evolution of the oxide thickness on the Ni-30(wt.%)Cr alloy immersed in various liquids with simplified compositions at 1150°C. Their simulations and experiments showed a good agreement, except when a depassivation phenomenon was occurring. Indeed, the model always predicts an increase of the oxide thickness and is thus unable to describe the depassivation. In a recent work [13], a link between depassivation and a decrease of the oxidation rate of the alloy due to a lack of the oxygen provided by the liquid has been highlighted.

Considering the dissolution of the chromia layer, it is assumed to be limited by the diffusion of chromium in the liquid, which leads to a parabolic dissolution kinetic. In a recent work [22], a complete model of dissolution of chromia based has been proposed: this model is based on chemical reactions, acid/base properties of the liquid and diffusion of the various chemical species. This complex model matches with the parabolic dissolution kinetic, in the case where the reactions are fast compared to the mass transport in the liquid.

The present work is a theoretical analysis of chromia-forming alloys corrosion in molten silicates. Based on the complete model of dissolution of chromia [22], a simplified version is proposed. The growth of the oxide layer by oxidation of the alloy in the liquid is added to the model. Simulations are performed to get prediction that can be experimentally verified. Thus, the focus was made on (i) the concentration profile of chromium in the quenched liquid (that can be measured by Electron Probe Micro Analysis) and (ii) the oxide thickness (that can be measured by Scanning Electron Microscopy). Eventually, the dependence between the oxide growth rate, the depassivation and the parameters of the model are presented in the last part of this work.

2. Equations

2.1. Dissolution of chromia in molten silicates

In a previous work, a model of the chromia dissolution in molten silicates has been developed [22]. This model was a synthesis of all the knowledge available in the literature

about this subject. The acid-base properties of the liquid were described by chemical reactions between Q^n (silica tetrahedra linked to n bridging oxygens) and the oxide ions O^{2-}. The oxidation states of chromium ions (Cr^{II}, Cr^{III} and Cr^{VI}) have been identified so as the reactions involved, thanks to various authors.

The accurate study of the complete model of dissolution of chromia [22] has shown that some parameters (e.g. the basicity of the liquid) are not affected by the dissolution of Cr, and that some others (e.g. diffusion of some species, some chemical reactions) can be neglected. The thorough identification of the relevant phenomena having a significant influence on the dissolution rate of chromia leads to simplify the system by considering (i) only the Cr^{III}, Cr^{VI} and O_2 species; (ii) the chemical reactions of dissolution of chromia into Cr^{III} and of oxidation of Cr^{III} into Cr^{VI} in the liquid; and (iii) that diffusion is the main mass transport mode. Based on these assumptions, the simplified model is thus developed in this article. The simulation performed in ref [22] (glass $25Na_2O$-$75SiO_2$) can be compared to the simplified model of dissolution presented in this work for the same parameters and the same conditions (1 h). For this purpose, the growth of the oxide was deactivated in the present corrosion model. The very good correlation between the results of the two simulations (for the Cr^{III}, Cr^{VI} and O_2 concentrations) in Fig. 1 validates the simplifications proposed in this work.

2.1.1. Chemical reaction of chromia dissolution

At the liquid/chromia interface, the dissolution of the chromia layer into Cr^{III} species is led by the following acid-base reaction [9].

$$\frac{1}{2}Cr_2O_{3\,cristal} \overset{dissolution}{\Longleftrightarrow} Cr^{III}O_X^{(3-2X)+} + \left(\frac{3}{2}-X\right)O^{2-} \qquad \text{eq. 3}$$

With $Cr^{III}O_X^{(3-2X)+}$ being the oxo-complex of Cr^{III} and O^{2-} the strong base of silica-based liquids. As the O^{2-} activity remains unchanged in the liquid during the dissolution [22], the mass action law associated to equation 3 is thus simplified due to the constant O^{2-} activity. Considering in first approximation the proportionality between activity and concentration, the following condition at the liquid/chromia interface (designated as “int”) can be expressed.

$$C_{Cr^{III}}\big|_{int} = S \qquad \text{eq. 4}$$

With S the solubility (mol m^{-3}) of Cr^{III} which is a value depending on the temperature and the glass composition.

2.1.2. Chemical reaction of Cr^{III} oxidation

In the liquid, the oxidation of Cr^{III} into Cr^{VI} requires O_2 as the oxidant. The following reaction has been proposed to describe this [9].

$$\mathrm{Cr^{III}O_X^{(3-2X)+}} + \frac{3}{4}\mathrm{O_2} + \left(\mathrm{Y} - \mathrm{X} - \frac{3}{2}\right)\mathrm{O^{2-}} \overset{\text{oxidation}}{\Longleftrightarrow} \mathrm{Cr^{VI}O_Y^{(2Y-6)-}} \qquad \text{eq. 5}$$

With $\mathrm{Cr^{VI}O_Y^{(2Y-6)-}}$ being the oxo-complex of Cr^{VI}. Based on the same simplifications than for equation 3 (i.e. a constant O^{2-} activity and proportionality between concentrations and activities), the following mass action law can be derived.

$$K = \frac{C_{Cr^{VI}}}{C_{Cr^{III}} \cdot {P_{O_2}}^{3/4}} \qquad \text{eq. 6}$$

With C_i the concentration of the chemical species i and P_{O_2} being the oxygen partial pressure (atm) in the atmosphere in equilibrium with the liquid. The reason why the oxygen activity is assimilated to its partial pressure in the atmosphere is due to the solubility plots previously established in many glass compositions [2,9,10,23], with all data given for various oxygen partial pressures in the atmosphere. Consequently, K (so as the S parameter) can be easily determined from these data.

In order to get a reaction rate, the oxygen partial pressure has to be translated in term of concentration. This can be achieved by assuming the equilibrium between the oxygen concentration in the liquid C_{O_2} and the partial pressure in the atmosphere P_{O_2}. The equilibrium constant is a Henry constant H (mol.m^{-3}.atm^{-1}).

$$H = \frac{C_{O_2}}{P_{O_2}} \qquad \text{eq. 7}$$

A reaction rate can thus be associated to the oxidation of Cr^{III}:

$$\xi = k\left(K \cdot H^{-3/4} \cdot C_{Cr^{III}} \cdot {C_{O_2}}^{3/4} - C_{Cr^{VI}}\right) \quad \text{eq. 8}$$

With ξ the reaction rate (mol m^{-3} s^{-1}) and k a kinetic coefficient (s^{-1}). The evolutions of the concentrations are equal to the reaction rates multiplied by the stoichiometric coefficients.

2.1.3. Equation system

The evolution of the concentrations of Cr^{III}, Cr^{VI} and O_2 in the liquid is due to the chemical reactions and to the mass transport. The complete model of dissolution of chromia [22] showed that Fickian diffusion is the most influencing mass transport mode of chromium and oxygen in the liquid. Thus, the flux $\vec{J_i}$ of any chemical species i (i = Cr^{III}, Cr^{VI}, O_2) is given by the well-known first Fick's law.

$$\vec{J_i} = -D_i \cdot \overrightarrow{\nabla(C_i)} \quad \text{eq. 9}$$

With D_i the diffusion coefficient (m^2 s^{-1}) and $\overrightarrow{\nabla(C_i)}$ the concentration gradient of i (mol m^{-4}). The evolution of the concentrations of Cr^{III}, Cr^{VI} and O_2 corresponds to both diffusion and chemical reactions. The following system can thus be formulated.

$$\frac{\partial C_{Cr^{III}}}{\partial t} = -\vec{\nabla} \cdot \overrightarrow{J_{Cr^{III}}} - \xi \quad \text{eq. 10}$$

$$\frac{\partial C_{Cr^{VI}}}{\partial t} = -\vec{\nabla} \cdot \overrightarrow{J_{Cr^{VI}}} + \xi \quad \text{eq. 11}$$

$$\frac{\partial C_{O_2}}{\partial t} = -\vec{\nabla} \cdot \overrightarrow{J_{O_2}} - \frac{3}{4}\xi \quad \text{eq. 12}$$

The equation 4 adds a condition for the liquid/chromia interface. The boundary conditions depend on the geometry of the spatial domain. The dissolution rate of the oxide is given by the following equation.

$$\left(\frac{de}{dt}\right)_{diss} = -\frac{V_m}{2}\left\|\overrightarrow{J_{Cr^{III}}}\right|_{int}\right\| \quad \text{eq. 13}$$

With $\left(\frac{de}{dt}\right)_{diss}$ being the loss rate of the oxide thickness (m.s^{-1}), V_m the molar volume of the oxide (for chromia 2.923 10^{-5} m^3.mol^{-1}) and $\left\|\overrightarrow{J_{Cr^{III}}}\right|_{int}\right\|$ the intensity of the Cr^{III} dissolution flux in the liquid (the vector being oriented from the oxide towards the liquid and $\| \|$ being the module/intensity of the vector). This last quantity can be calculated from the following expression.

$$-\vec{\nabla} \cdot \overrightarrow{J_{Cr^{III}}}\Big|_{int} = \frac{\partial C_{Cr^{III}}}{\partial t}\Big|_{int} \quad \text{eq. 14}$$

2.2. Oxidation of the alloy

According to the well-known works of Tammann [15] and Wagner [16,17], the growth of an oxide layer on an alloy is driven by the diffusion of defects through the layer. The oxide growth rate is given by the following equation.

$$\left(\frac{de}{dt}\right)_{form} = \frac{k_p}{e} \quad \text{eq. 15}$$

With k_p the parabolic growth constant of the oxide which depends on the nature of the defect driving the oxide growth. In molten silicates, considering that the oxygen activity is lower than in the overhanging atmosphere [24] and that the temperature is usually higher than those applied by Tsai *et al*. [4], the main defect of the chromia layer can be assumed to be interstitial chromium. This statement is a simplified version of the physic and chemistry of the high temperature oxidation, but it allows to formulate the evolution of the parabolic growth constant of chromia (k_p) *vs.* the oxygen pressure/activity in the external medium according to:

$$k_p = A\left(P_{O_2}^{al/ox\,-3/4} - P_{O_2}^{ox/ex\,-3/4}\right) \quad \text{eq. 16}$$

With A a constant depending on the temperature, $P_{O_2}^{al/ox}$ the oxygen partial pressure at the oxide/alloy interface and $P_{O_2}^{ox/ex}$ the oxygen pressure at the oxide/exterior interface. By

changing the oxygen pressure by concentration and rewriting the equation 16, the following equation can be found.

$$k_p = {k_p}^{ref}\left(1 - \left(\frac{C_{O_2}|_{int}}{{C_{O_2}}^{ref}}\right)^{-3/4}\right) \qquad \text{eq. 17}$$

In this expression ${k_p}^{ref}$ ($m^2.s^{-1}$) is the value of k_p at high oxygen pressure and ${C_{O_2}}^{ref}$ is the oxygen partial pressure at the oxide/alloy interface expressed as an equivalent concentration. If the oxygen concentration in the liquid $C_{O_2}|_{int}$ is close to ${C_{O_2}}^{ref}$, the oxide growth is slown down until it stops at $C_{O_2}|_{int} = {C_{O_2}}^{ref}$. A concentration $C_{O_2}|_{int}$ below the concentration ${C_{O_2}}^{ref}$ does not allow the growth of the oxide (the oxidation reaction is thermodynamically not favored). In the other case, the oxide growth follows the equation 15 with a parabolic growth constant close to ${k_p}^{ref}$.

The growing oxide layer requires an oxygen supply from the liquid according to the following oxidation reaction of chromium from the alloy.

$$2Cr + \frac{3}{2}O_2 \Leftrightarrow Cr_2O_3 \qquad \text{eq. 18}$$

Thus, the oxygen flux in the liquid is linked to the oxide growth rate by the following equation (the vector $\overrightarrow{J_{O_2}}|_{int}$ being oriented from the liquid towards the oxide).

$$\left\|\overrightarrow{J_{O_2}}|_{int}\right\| = \frac{3}{2V_m}\cdot\frac{k_p}{e} \qquad \text{eq. 19}$$

The evolution of the oxide thickness is given by the following equation (eq. 13 for dissolution and eq. 15 for formation).

$$\frac{de}{dt} = \frac{k_p}{e} - \frac{V_m}{2}\left\|\overrightarrow{J_{Cr^{III}}}|_{int}\right\| \qquad \text{eq. 20}$$

In the present development, the chromium depletion in the alloy is not considered. Experimental results of pre-oxidized Ni-30Cr immersion in molten silicates [14] showed that the chromium depletion is similar whether the alloy is immersed or simply subject to

oxidation in air [5-6]. This would suggest that the diffusion of chromium in the alloy is sufficiently rapid to ensure the growth of the chromium layer under these conditions.

2.3. Parameters of the model and 1D example

The above equations allow to describe the formation/dissolution of the growing oxide scale by three partial differential equations for the evolution of the Cr^{III}, Cr^{VI} and O_2 concentrations in the liquid (equations 10, 11 and 12 respectively), two boundary conditions at the liquid/chromia interface for the dissolution of chromia and its growth (equations 4 and 19 respectively) and one ordinary equation for the evolution of the chromia layer thickness (equation 20). The equation system can be simplified by introducing dimensionless parameters. The dimensionless time $\hat{t}$, length $\hat{x}$, diffusion/oxidation ratio $\widehat{D}$ and diffusion coefficients ratios R^i are given by the following equations (every dimensionless quantity are given with a hat).

$$\hat{t} = k \cdot t \qquad \hat{x} = \sqrt{\frac{k}{k_p^{ref}}} \cdot x \qquad \widehat{D} = \frac{D_{Cr^{III}}}{k_p^{ref}} \qquad R^i = \frac{D_i}{D_{Cr^{III}}} \qquad \text{eq. 21}$$

With k the kinetic constant of the Cr^{III}/Cr^{VI} oxidation reaction, k_p^{ref} the parabolic growth constant of the oxide in high oxygen pressure/concentration and $D_{Cr^{III}}$ the diffusion coefficient of Cr^{III} in the liquid. In one dimension the evolutions of the Cr^{III}, Cr^{VI} and O_2 concentrations in the liquid are given by the following system.

$$\frac{\partial C_{Cr^{III}}}{\partial \hat{t}} = \widehat{D} \cdot \frac{\partial^2 C_{Cr^{III}}}{\partial \hat{x}^2} - \left(K \cdot H^{-3/4} \cdot C_{Cr^{III}} \cdot {C_{O_2}}^{3/4} - C_{Cr^{VI}}\right) \qquad \text{eq. 22}$$

$$\frac{\partial C_{Cr^{VI}}}{\partial \hat{t}} = \widehat{D} \cdot R^{Cr^{VI}} \cdot \frac{\partial^2 C_{Cr^{VI}}}{\partial \hat{x}^2} + \left(K \cdot H^{-3/4} \cdot C_{Cr^{III}} \cdot {C_{O_2}}^{3/4} - C_{Cr^{VI}}\right) \qquad \text{eq. 23}$$

$$\frac{\partial C_{O_2}}{\partial \hat{t}} = \widehat{D} \cdot R^{O_2} \cdot \frac{\partial^2 C_{O_2}}{\partial \hat{x}^2} - \frac{3}{4}\left(K \cdot H^{-3/4} \cdot C_{Cr^{III}} \cdot {C_{O_2}}^{3/4} - C_{Cr^{VI}}\right) \qquad \text{eq. 24}$$

The initial concentration distribution consists of a concentration of zero for Cr^{III} and Cr^{VI}, and a homogeneous O_2 concentration given by the Henry's constant H and the partial pressure of oxygen in the atmosphere (equation 7).

The boundary conditions at the position x = 0 (chromia/liquid interface) are the following ones.

$$C_{Cr^{III}}\big|_{x=0} = S \qquad \text{eq. 25}$$

$$-\widehat{D} \cdot R^{O_2} \cdot \frac{\partial C_{O_2}}{\partial \hat{x}}\bigg|_{x=0} = \frac{3}{2V_m} \cdot \frac{\hat{k}_p}{\hat{e}} \qquad \text{eq. 26}$$

The Cr^{III} and Cr^{VI} diffusion fluxes in the liquid through the limit x = 0 are set to zero as these two species cannot diffuse into the chromia layer. At the other limit ($x \rightarrow \infty$) the concentrations are unchanged. The system is described by the following parameters: the Cr^{III} solubility S, the Cr^{III}/Cr^{VI} oxidation constant K, the Henry constant H, the diffusion/oxidation ratio $\widehat{D}$, the diffusion ratio $R^{Cr^{VI}}$ and R^{O_2}. The evolution of the oxide thickness is given by the dimensionless form of the equation 20:

$$\frac{d\hat{e}}{d\hat{t}} = \frac{\hat{k}_p}{\hat{e}} - \frac{V_m}{2}\left\|\overrightarrow{\hat{J}_{Cr^{III}}}\big|_{int}\right\| \qquad \text{eq. 27}$$

3. Simulation

3.1. Solver

The equation system is solved by using a finite volume with a simple unidimensional schema. The space is meshed by elementary segments. The concentrations and the time derivatives of concentrations are defined at the middle of the segments. The fluxes are defined at the borders of each segment. To maintain the semi-infinite assumption during the calculation, the length of the spatial domain is defined by the following equation.

$$\hat{L}_{tot} = 3 \cdot \sqrt{2 \cdot max\left(\widehat{D} \cdot R^i\right) \cdot \hat{t}_{final}} \qquad \text{eq. 28}$$

The above equation ensures that none of the concentrations will change far from the interface.

The integration over time is performed using a simple Euler explicit method. In order to control the accuracy of the numerical schema, the time step is calculated in order to let the integrated function increase or decrease from a fraction of its value, this fraction being the relative tolerance (*reltol*). If the function is close to zero, the step time will be also close to zero and consequently stop the integration. Thus, an absolute tolerance (*abstol*) has to be set in order to avoid this possibility. The step time is calculated using the following formula.

$$\delta t = min\left((reltol \cdot |u(t)| + abstol)/\left|\frac{\partial u}{\partial t}(t)\right|\right) \quad \text{eq. 29}$$

This method has been successfully used in a previous work to simulate the dissolution of chromia in silica-based liquids [22]. The accuracy chosen for the simulation is also used to define ${C_{O_2}}^{ref}$ which intervenes in the expression of k_p (equation 17). Physically, this quantity is defined by the equilibrium O_2 activity/pressure at the oxide/alloy interface. For chromia/pure chromium at 1100 °C, this value is around 10^{-20} atm [25]. This value is too low in comparison to the concentrations encountered in the glass (hundreds of mol m^{-3} for the solubility of Cr^{III}) and might cause digit issues during the numerical calculation. To prevent this problem, ${C_{O_2}}^{ref}$ is set to a value without physical meaning, low enough in comparison to the other concentrations in the liquid but high enough to avoid the loss of digits. The value is set to $10 \cdot abstol/reltol$. This expression ensures that the O_2 concentration at the liquid/chromia interface will not oscillate around ${C_{O_2}}^{ref}$ because of the limited accuracy of the simulation which would result in a negative k_p with no physical meaning. For every simulation presented in this work, *reltol* = 0.001 and *abstol* = 0.00001 mol.m^{-3}, which gives ${C_{O_2}}^{ref}$ = 0.1 mol m^{-3}.

3.2. Modeling of the corrosion of Ni-30Cr in the $25Na_2O$-$75SiO_2$ liquid

The $25Na_2O$-$75SiO_2$ liquid has a simple composition for which the parameters involved in the simulation are known. S and K can be calculated from the solubility measurements performed by Khedim *et al.* [9]. H, $\widehat{D}$, $R^{Cr^{VI}}$ and R^{O_2} can be calculated from the work of Schmucker *et al.* [5,6] and from our previous work [22]. The set of parameters used for the simulation of the evolution of the oxide thickness on a Ni-30Cr alloy immersed in the $25Na_2O$-$75SiO_2$ liquid at 1150 °C is given in Table 1.

The simulation was performed for 1000 $\hat{t}$ with 8.39 $\hat{x}$ pre-oxide thickness. The results are presented using the dimensionless distance and time in order to focus on the shape of the diffusion profiles and thickness evolution. By using k_p^{ref} = 5 10^{-12} cm^2 s^{-1} [5,6] and k = 0.01 s (arbitrarily chosen but fast enough to represent a high temperature reaction kinetic), the dimensionless length $\hat{x}$ is equal to 0.224 µm and 1$\hat{t}$ represents 100 s. With these values the simulation time of 1000 $\hat{t}$ corresponds to 27.77 h and the pre-oxide is 2 µm thick.

The diffusion profiles of Cr^{III}, Cr^{VI} and O_2 given in Figure 2 present noticeable features: the O_2 concentration at the liquid/chromia interface is low because of the chromia scale growth, and in result, the Cr^{III} is poorly oxidized in Cr^{VI}. The total chromium concentration at this interface thus corresponds to the solubility S of Cr^{III}. This fact was confirmed by Schmucker *et al.* [14] for the Ni-30Cr alloy immersed 51 h in the $25Na_2O$-$75SiO_2$. Far from the interface, the oxygen concentration increases to reach the value imposed by the Henry constant and the external O_2 partial pressure (400 mol m^{-3}). As a result, at distances from 0 to 250 $\hat{x}$, the Cr^{VI} concentration increases and reaches a maximum before continuously decreasing. As Cr^{III} is diffusing, its concentration decreases when the distance from the interface increases. Consequently, the Cr^{VI} concentration also decreases from 250 $\hat{x}$ to the core of the liquid because of the low Cr^{III} concentration.

Figure 3 corresponds to the diffusion profiles of total chromium (Cr^{III} + Cr^{VI}) and O_2 at various times. Despite the specific shape of the Cr^{VI} concentration profile, the shape of the total chromium concentration profile can still be assimilated to a classical complementary error function (*erfc*) solution of the second Fick law for semi-infinite diffusion with constant concentration at the finite limit. The evolution with $\sqrt{t}$ can be noticed and the concentrations at the interface converge in all the cases considered here, which corresponds to a parabolic regime.

The evolution of the oxide thickness (Figure 4a) starts with a light decrease at the beginning of the simulation from 0 to 6 $\hat{t}$, before exhibiting a global parabolic shape. This is coherent with the formation/dissolution equation as shown by Gheno *et al.* [20]: the formation is slowed down by the pre-oxide while the dissolution is accelerated by the absence of dissolved chromium in the liquid. Then, the thickness increases quickly from 6 to 50 $\hat{t}$ before tending to a slow parabolic growth. In order to analyze the evolution of the system, parabolic quantities are defined as follows.

$$\hat{g} = \hat{e} \cdot \frac{d\hat{e}}{d\hat{t}} \qquad \text{eq. 30}$$

$$\hat{k}_d = 2\hat{t}\left(\frac{V_m}{2}\left\|\overrightarrow{\hat{J}^{diss}_{Cr^{III}}}\Big|_{x=0}\right\|\right)^2 \qquad \text{eq. 31}$$

$\hat{g}$ represents the dimensionless global parabolic growth constant, $\hat{k}_d$ is the dimensionless parabolic dissolution constant and $\hat{k}_p$ defined by the dimensionless version of the equation 17 completes this description. The evolution of these quantities during the simulation is given Figure 4b. Three regimes can be noted. During the first moments of the immersion (from 0 up to 30 $\hat{t}$), the oxidation parabolic constant $\hat{k}_p$ remains equal to 1 meaning that the oxygen concentration at the liquid/chromia interface is high enough to sustain the oxidation of the alloy. The value of the dissolution parabolic constant $\hat{k}_d$ decreases during this step. A thorough analysis of the oxygen concentration close to the interface shows its decrease during this step. Cr^{III} is first oxidized in Cr^{VI}, then considering the consumption of the O_2 by the growing oxide layer, Cr^{VI} can be reduced in Cr^{III}, thus decreasing the quantity of Cr^{III} brought by the chromia dissolution, and so $\hat{k}_d$. This phenomenon might explain the oxide needles observed on the pre-oxidized Ni-30Cr alloy immersed for a short duration [13]. The second step (from 30 $\hat{t}$ up to > 1000 $\hat{t}$) corresponds to a transition. The three quantities $\hat{g}$, $\hat{k}_d$ and $\hat{k}_p$, converge to stable values. $\hat{k}_p$ decreases due to the insufficient O_2 supply from the liquid: the kinetic growth of the oxide is then controlled by O_2 diffusion in the liquid. The final step is reached when the three parabolic quantities have converged to stable values and are then linked by the equation 2: this step is the permanent parabolic regime. The transition time between the initial step and the permanent parabolic regime was found to depend on the pre-oxide thickness. With a thinner pre-oxide, the permanent parabolic regime is quickly reached.

3.3. Influence of the dissolved oxygen

Among the parameters used for this simulation, the concentration of dissolved oxygen or the Henry constant (eq. 7) seems to be the most important as it can determine the oxide growth rate. However, this parameter is also the less known. Electrochemical measurements performed by Tilquin *et al*. [26] showed that the O_2 system in molten silicates is complex with

possibly various form of oxygen. The O_2 activity in the liquid can be determined by potentiometry [24,27–29], but the link between activity and concentration is not clear. Solubility of N_2 measured in the same kind of system [30] showed that the dissolved gas mass can reach 0.5 %, which represents several hundreds of $mol.m^{-3}$. The Henry constant of 2000 $mol.m^{-3}.atm^{-1}$ used in this work is relatively coherent but not certain.

Simulation was performed with the set of parameters presented in Table 1, but for various H values. The evolutions of the oxide thickness are given Figure 5a, the diffusion profiles of the total chromium in the liquid are given Figure 5b. The oxide thickness is continuously decreasing in the case of the H = 500 mol m^{-3} atm^{-1}, following a negative $\hat{g}$ value. In the end the oxide is completely dissolved by the liquid. This corresponds to a depassivation phenomenon as presented in the introduction of this work. The oxygen concentration is too low to ensure an oxide growth rate faster than its dissolution. Consequently, the chromia layer is not stable and is eventually dissolved. This scenario was used in a previous work to explain the depassivation phenomenon [13] and seems to be confirmed by this model. The growth rate of the oxide increases with H when $500 < H < 4500$ mol m^{-3} atm^{-1}. For H = 4500 mol m^{-3} atm^{-1}, the obtained thickness and growth rate is also coherent with the value obtained by Schmucker [21] ($g = 2\ 10^{-12}$ cm^2 s^{-1}) in the same liquid at 1150 °C. The analysis of the corresponding chromium diffusion profiles in the liquid (Figure 5b) shows that the quantity of dissolved chromium is constant for H comprised between 500 and 4500 mol m^{-3} atm^{-1}. In the case of H = 5500 mol m^{-3} atm^{-1}, the oxide thickness is lower than for H = 4500 mol m^{-3} atm^{-1}. In this case, the growing oxide does not consume all the dissolved O_2, and thus the oxidation of Cr^{III} in Cr^{VI} is favored. Consequently, the quantity of dissolved chromium becomes higher than for H comprised between 500 and 4500 mol m^{-3} atm^{-1}.

4. Parabolic regime, passivation and depassivation

It appears from the results presented in the above section that the relation between the depassivation and the oxide growth and the parameter H of the model are intricate. To ease the comprehension of the system, simulation has been performed for conditions ensuring that the simulation has reached the permanent parabolic regime, which are a duration of 14 h and a pre-oxide thickness of 2 nm. Simulations are performed by varying only one of the six

parameters (i.e. S, K, H, $\widehat{D}$, $R^{Cr^{VI}}$ and R^{O_2}), the other parameters being equal to the values in Table 1. The final values of $\hat{g}$, $\hat{k}_p$ and $\hat{k}_d$ are extracted from the simulation. The six obtained graphs are given in Figure 6. Each graph corresponds to the evolution of $\hat{g}$, $\hat{k}_p$ and $\hat{k}_d$ in the permanent parabolic regime *vs.* one of the six parameters.

It appears from these results that three domains can be distinguished. The "intrinsic oxide growth" domain that can be noticed in Figure 6c and 6d corresponds to a passive domain with an oxide growth limited by the intrinsic value of k_p ($\hat{k}_p \approx 1$): the O_2 concentration in the liquid is high enough to support the oxide growth rate. The "limited oxide growth" domain corresponds to a passive state with an oxide growth rate limited by the O_2 supply from the liquid ($0 < \hat{k}_p < 1$). The "no passive state" domain corresponds to the active corrosion domain (or the depassivation domain) as in this domain even a pre-oxidized alloy ends up in a depassivated state: the O_2 supply from the liquid is too low to ensure an oxide growth fast enough to overcome the oxide dissolution ($\hat{k}_p = 0$).

From Figure 6 and the evolution of $\hat{g}$ with the six parameters, it can be stated that solubility and oxidation of Cr^{III} (i.e. high S and K values) are always detrimental for the alloy protection as they decrease the global parabolic formation constant $\hat{g}$ (Figures 6a and 6b) by implying a faster oxide dissolution rate ($\hat{k}_d$ increase). A higher chromium concentration in the liquid also implies a higher O_2 consumption by the Cr^{III} oxidation into Cr^{VI}, which directly decreases the oxygen supply for the oxide formation ($\hat{k}_p$ decrease).

High $R^{Cr^{VI}}$ and R^{O_2} values (Figures 6c and 6d) increase the corrosion protection of the alloy as they increase $\hat{g}$. In the case of R^{O_2}, this is not a surprising result as it increases the O_2 supply towards the growing oxide scale. In the case of $R^{Cr^{VI}}$, this result is unexpected but can be explained by the shape of the Cr^{VI} concentration profile as seen in Figure 1. In the "limited oxide growth" domain the low O_2 concentration at the oxide/liquid interface causes the rising and descending shape of the Cr^{VI} concentration profile. As a result, the flux of Cr^{VI} is oriented towards the oxide scale close to the interface. By diffusing in this direction, Cr^{VI} encounters an area depleted in O_2, and is thus reduced into Cr^{III} and releasing O_2 that can be used to grow the oxide scale. Cr^{VI} transports the O_2 from an oxygen-rich area (far from the interface) towards the interface.

The cases of H and $\widehat{D}$ (Figures 6e and 6f) are complex. Low H values are detrimental as the O_2 concentration in the liquid becomes too low to ensure the growth of the oxide. But high H values are also detrimental as more oxygen is available in the liquid to oxidize Cr^{III} into Cr^{VI}, and thus increase $\hat{k}_d$. There is an optimum value of H for which $\hat{k}_d$ is minimized and $\hat{k}_p$ is maximized. The same phenomenon occurs for $\widehat{D}$. For low $\widehat{D}$ values the oxygen supply is low, and the oxide growth is limited. For higher values, the oxygen supply is no more limiting ($\hat{k}_p \approx 1$), but the dissolution rate of the oxide keeps increasing.

Among the six parameters, those linked to the dissolved oxygen, i.e. R^{O_2} and H, have the most significant influence on the oxide growth rate as a small variation of these parameters can drastically change the corrosion state and the oxide growth rate.

Conclusion

The model presented in this work allowed to explain the depassivation of chromia forming alloys in molten silicates. This phenomenon is caused by a lack of O_2 supply in the liquid towards the growing oxide scale. The dissolution overcomes the formation of the oxide resulting in a complete dissolution of the passive layer. Six parameters were identified (i.e. the Cr^{III} solubility S, the Cr^{III}/Cr^{VI} oxidation constant K, the henry constant H, the diffusion/oxidation ratio $\widehat{D}$, the diffusion ratio $R^{Cr^{VI}}$ and R^{O_2}), and simulations were performed in order to determine the specific influence of each parameter on the oxide growth rate. Three domains were defined: (i) a first one in which the oxide growth is impossible and leads to the depassivation of the alloy, (ii) a second one in which the oxide growth is possible but limited by the O_2 supply from the liquid, and (iii) a third one in which the oxide growth is only limited by its own parabolic growth constant. The relations between the six parameters, the three domains and the oxide growth rate in the liquid are intricate but an overview has been proposed in this work. It appears that the conditions favoring the depassivation of the protected alloy immersed in a silica-based liquid are a low O_2 concentration in the liquid, a low O_2 diffusivity, and a high limit of solubility of chromia.

This model is simple and requires a relatively low number of parameters to simulate the corrosion of a chromia-forming alloy. Consequently, it can be easily applied in many processes in order to simulate and optimize the protection against active corrosion of alloys.

Data availability

The raw/processed data required to reproduce these findings cannot be shared at this time due to technical or time limitations.

References

[1] Sengupta P. Interaction study between nuclear waste-glass melt and ceramic melter bellow liner materials. J Nucl Mater 2011;411:181–4. https://doi.org/10.1016/j.jnucmat.2011.01.122.

[2] Schmucker E, Petitjean C, Panteix P-J, Martinelli L, Ben Lagha S, Vilasi M. Correlation between chromium physicochemical properties in silicate melts and the corrosion behavior of chromia-forming alloy. J Nucl Mater 2018;510:100–8. https://doi.org/10.1016/j.jnucmat.2018.07.059.

[3] Ecer GM, Meier GH. Oxidation of high-chromium Ni-Cr alloys. Oxid Met 1979;13:119–58. https://doi.org/10.1007/BF00611976.

[4] Tsai SC, Huntz AM, Dolin C. Growth mechanism of Cr2O3 scales: oxygen and chromium diffusion, oxidation kinetics and effect of yttrium. Mater Sci Eng A 1996;212:6–13. https://doi.org/10.1016/0921-5093(96)10173-8.

[5] Schmucker E, Petitjean C, Martinelli L, Panteix P-J, Ben Lagha S, Vilasi M. Oxidation of Ni-Cr alloy at intermediate oxygen pressures. I. Diffusion mechanisms through the oxide layer. Corros Sci 2016;111:474–85. https://doi.org/10.1016/j.corsci.2016.05.025.

[6] Schmucker E, Petitjean C, Martinelli L, Panteix P-J, Lagha B, Vilasi M. Oxidation of Ni-Cr alloy at intermediate oxygen pressures. II. Towards the lifetime prediction of alloys. Corros Sci 2016;111:467–73. https://doi.org/10.1016/j.corsci.2016.05.024.

[7] Manfredo LJ, McNally RN. Solubility of Refractory Oxides in Soda-Lime Glass. J Am Ceram Soc 1984;67:C-155-C–158. https://doi.org/10.1111/j.1151-2916.1984.tb19178.x.

[8] Kim C-W, Choi K, Park J-K, Shin S-W, Song M-J. Enthalpies of Chromium Oxide Solution in Soda Lime Borosilicate Glass Systems. J Am Ceram Soc 2001;84:2987–90. https://doi.org/10.1111/j.1151-2916.2001.tb01125.x.

[9] Khedim H, Podor R, Panteix PJ, Rapin C, Vilasi M. Solubility of chromium oxide in binary soda-silicate melts. J Non-Cryst Solids 2010;356:2734–41. https://doi.org/10.1016/j.jnoncrysol.2010.09.045.

[10] Abdullah TK, Petitjean C, Panteix P-J, Rapin C, Vilasi M, Hussain Z, et al. Dissolution equilibrium of chromium oxide in a soda lime silicate melt exposed to oxidizing and reducing atmospheres. Mater Chem Phys 2013;142:572–9. https://doi.org/10.1016/j.matchemphys.2013.07.055.

[11] Abdullah TK, Petitjean C, Panteix P-J, Mathieu S, Rapin C, Vilasi M, et al. Electrochemical characterization of chromia-and alumina-forming nickel-based superalloys in molten silicates. Appl Surf Sci 2016;360:510–8.

[12] Abdullah TK, Petitjean C, Panteix PJ, Schmucker E, Rapin C, Vilasi M. Corrosion of Pure Cr and Ni–30Cr Alloy by Soda–Lime–Silicate Melts: Study of Simplified Systems. Oxid Met 2016;85:3–16. https://doi.org/10.1007/s11085-015-9571-2.

[13] Szczepan V, Petitjean C, Panteix PJ, Vilasi M. Corrosion and depassivation of a chromia-forming Ni-based alloy in the 0.75Na2O-B2O3-2.75SiO2 melt. Corros Sci 2020:108579. https://doi.org/10.1016/j.corsci.2020.108579.

[14] Schmucker E, Szczepan V, Martinelli L, Petitjean C, Panteix PJ, Ben Lagha S, et al. Kinetic modelling of Cr2O3 growth on a Ni-30Cr alloy in silicate melts. Corros Sci 2020;175:108873. https://doi.org/10.1016/j.corsci.2020.108873.

[15] Tammann G. Über Anlauffarben von Metallen. Z Für Anorg Allg Chem 1920;111:78–89. https://doi.org/10.1002/zaac.19201110107.

[16] Wagner C. Beitrag zur Theorie des Anlaufvorgangs. Z Für Phys Chem 1933;21B. https://doi.org/10.1515/zpch-1933-2105.

[17] Wagner C. Beitrag zur Theorie des Anlaufvorganges. II. Z Für Phys Chem 1936;32B:447–62. https://doi.org/10.1515/zpch-1936-3239.

[18] Gheno T, Meier GH, Gleeson B. High Temperature Reaction of MCrAlY Coating Compositions with CaO Deposits. Oxid Met 2015;84:185–209. https://doi.org/10.1007/s11085-015-9550-7.

[19] Gheno T, Gleeson B. Kinetics of Al2O3-Scale Growth by Oxidation and Dissolution in Molten Silicate. Oxid Met 2017;87:527–39. https://doi.org/10.1007/s11085-016-9686-0.

[20] Gheno T, Lindwall G. On the Simulation of Composition Profiles in NiCoCrAl Alloys During Al2O3 Scale Growth in Oxidation and Oxidation–Dissolution Regimes. Oxid Met 2019;91:243–57. https://doi.org/10.1007/s11085-018-9877-y.

[21] Schmucker E. Compréhension et modélisation des mécanismes de corrosion des alliages chromino-formeurs dans les verres nucléaires. Thesis. Nancy: Univerité de lorraine; 2016.

[22] Szczepan V, Brix F, Petitjean C, Panteix PJ, Vilasi M. A new modeling of the dissolution of chromia in Na2O-SiO2 liquids. J Non-Cryst Solids 2020;545:120153. https://doi.org/10.1016/j.jnoncrysol.2020.120153.

[23] Khedim H, Podor R, Rapin C, Vilasi M. Redox-Control Solubility of Chromium Oxide in Soda-Silicate Melts. J Am Ceram Soc 2008;91:3571–9. https://doi.org/10.1111/j.1551-2916.2008.02692.x.

[24] Rüssel C, Kohl R, Schaeffer HA. Interaction between oxygen activity of Fe2O3 doped soda-lime-silica glass melts and physically dissolved oxygen 1988;61:209–13.

[25] Roine A. HSC Chemistry for Windows. Outokumpu Res Oy Pori 1994.

[26] Tilquin J-Y, Glibert J, Claes P. Anodic polarization in molten silicates. J Non-Cryst Solids 1995;188:266–74. https://doi.org/10.1016/0022-3093(95)00198-0.

[27] Douglas RW, Nath P, Paul A. Oxygen Ion Activity and Its Influence on Redox Equilibrium in Glasses. Phys Chem Glas 1965;6:216.

[28] Baucke F, Pfeiffer T, Biedenbender S, Roth G, Werner R-D. Reference electrode for electrochemical determination of oxygen partial pressure in an ionic melt, 1996.

[29] Perkins RA. Oxygen sensor and method for determining the oxygen activity in molten glass, 1982.

[30] Mulfinger H-O. Physical and Chemical Solubility of Nitrogen in Glass Melts. J Am Ceram Soc 1966;49:462–7. https://doi.org/10.1111/j.1151-2916.1966.tb13300.x.

Tables

Table 1: Set of parameters used to simulate the evolution of the chromia thickness on the Ni-30Cr alloy immersed in the $25Na_2O$-$75SiO_2$ at 1150 °C.

Parameters	Values
S	412 $mol.m^{-3}$
K	7.019 $atm^{-0.75}$
H	2000 $mol.m^{-3}.atm^{-1}$
$\widehat{D}$	2700
$R^{Cr^{VI}}$	0.5385
R^{O_2}	2.069

Figure captions

Figure 1: Simulation of the concentration profiles of Cr^{III}, Cr^{VI} and O_2 performed with the complete model of dissolution (ref [22]) and the present dissolution model (growth of the oxide deactivated). Case of the dissolution of chromia in 25Na2O-75SiO2 at 1150°C.

Figure 2: Simulated concentration profiles of Cr^{III} (green), Cr^{VI} (brown) and O_2 (red) in $25Na_2O$-$75SiO_2$ for Ni-30Cr immersed for 1000 $\hat{t}$, a pre-oxide of 8.39 $\hat{x}$, and the parameters available in Table 1 (1150 °C).

Figure 3: Simulated concentration profiles of Cr and O_2 in $25Na_2O$-$75SiO_2$ for Ni-30Cr immersed for 200, 400, 600, 800 and 1000 $\hat{t}$, a pre-oxide of 8.39 $\hat{x}$, and the parameters available in Table 1 (1150 °C).

Figure 4: Simulation of the immersion of Ni-30Cr in $25Na_2O$-$75SiO_2$, a pre-oxide of 8.39 $\hat{x}$ and the parameters available in Table 1 (1150 °C). (a): evolution of the oxide thickness; (b): Evolution of the parabolic constants of the system, $\hat{k}_p$ (green), $\hat{k}_d$ (red) and $\hat{g}$ (blue)

Figure 5: Simulated (a) oxide thickness on Ni-30Cr immersed in $25Na_2O$-$75SiO_2$ and (b) concentration profiles of Cr and O_2 in the liquid, for a pre-oxide of 8.39 $\hat{x}$, and the parameters available in Table 1 (1150 °C) and H = 500, 1500, 2500, 3500, 4500 and 5500 $mol.m^{-3}.atm^{-1}$.

Figure 6: Evolution of $\hat{k}_p$ (green), $\hat{k}_d$ (red) and $\hat{g}$ (blue) in the permanent parabolic regime for a duration of 500 $\hat{t}$, a pre-oxide of 0.01 $\hat{x}$ and the set of parameters available in Table 1; (a): as a function of Cr^{III} solubility S; (b): as a function of Cr^{III}/Cr^{VI} reaction constant K; (c) as a function of the diffusion/oxidation ratio $\widehat{D}$; (d) as a function of H; (e) as a function of $R^{Cr^{VI}}$; (f) as a function of R^{O_2}.

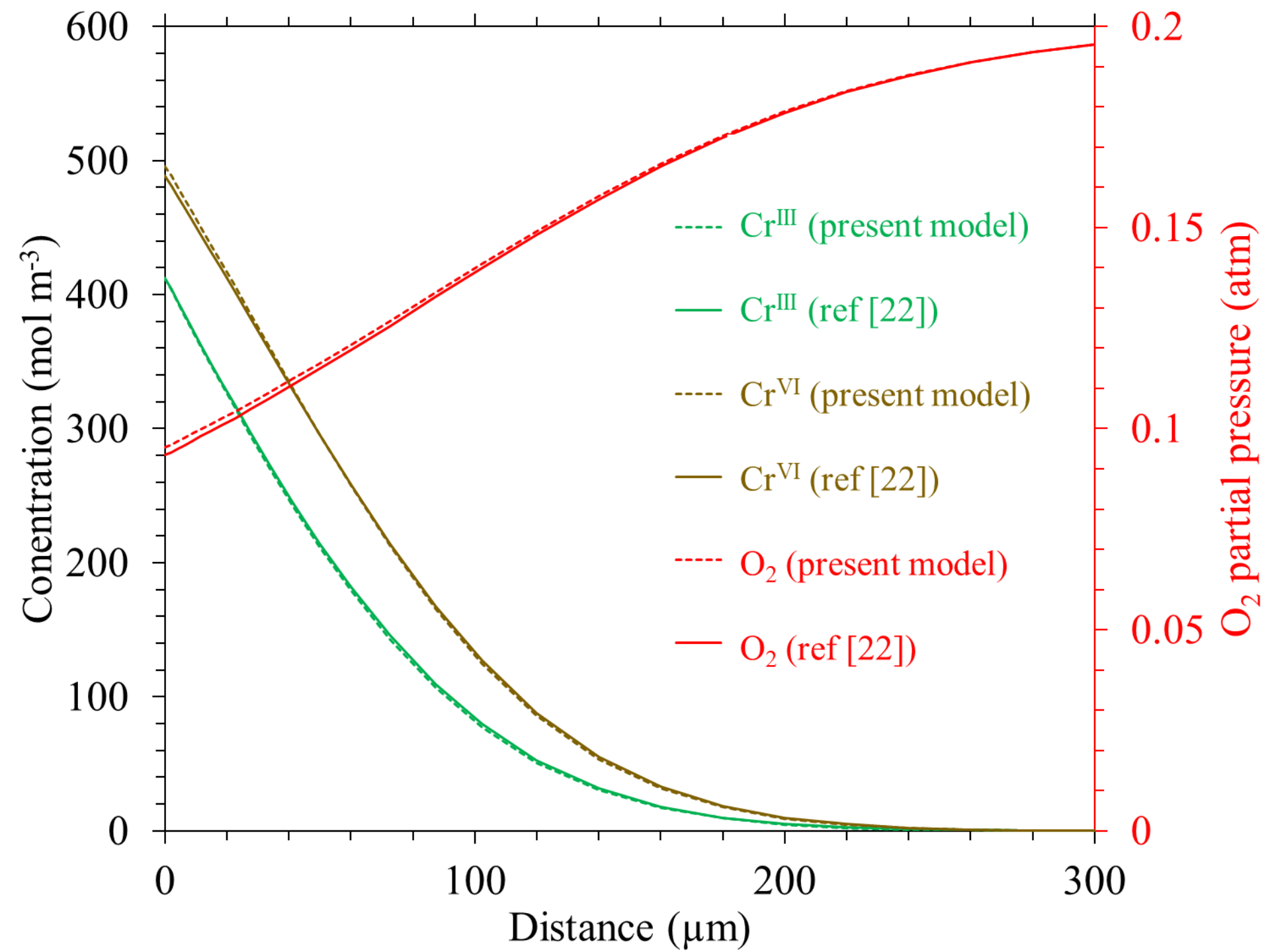
600
500
400
300
200
100
0
Conentration (mol m-3)
0.2
0.15
0.1
0.05
0
O2 partial pressure (atm)
0
100
200
300
Distance (μm)
CrIII (present model)
CrIII (ref [22])
CrVI (present model)
CrVI (ref [22])
O2 (present model)
O2 (ref [22])

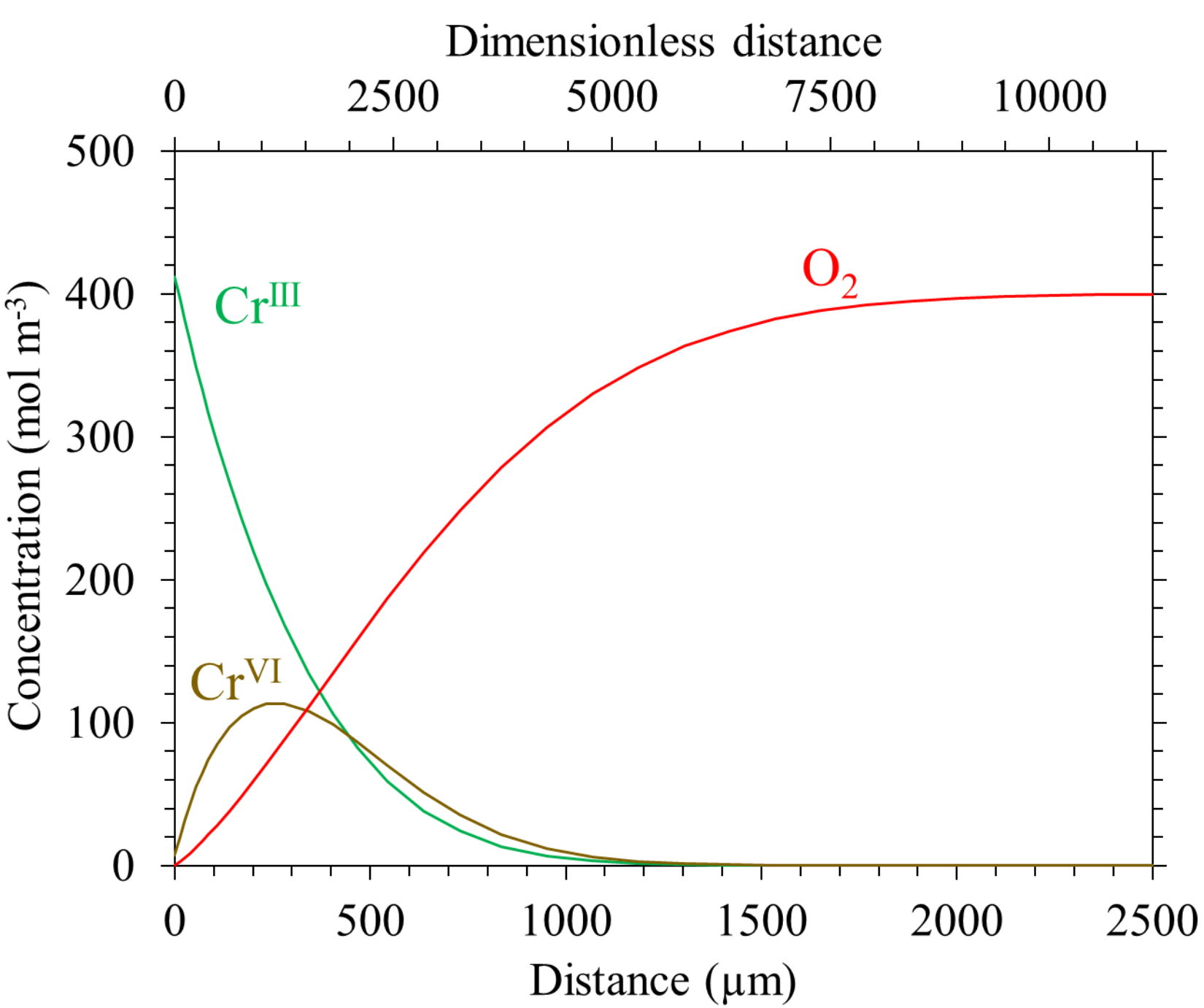
Dimensionless distance
0
2500
5000
7500
10000
500
400
300
200
100
0
Concentration (mol m-3)
CrIII
O2
CrVI
0
500
1000
1500
2000
2500
Distance (μm)

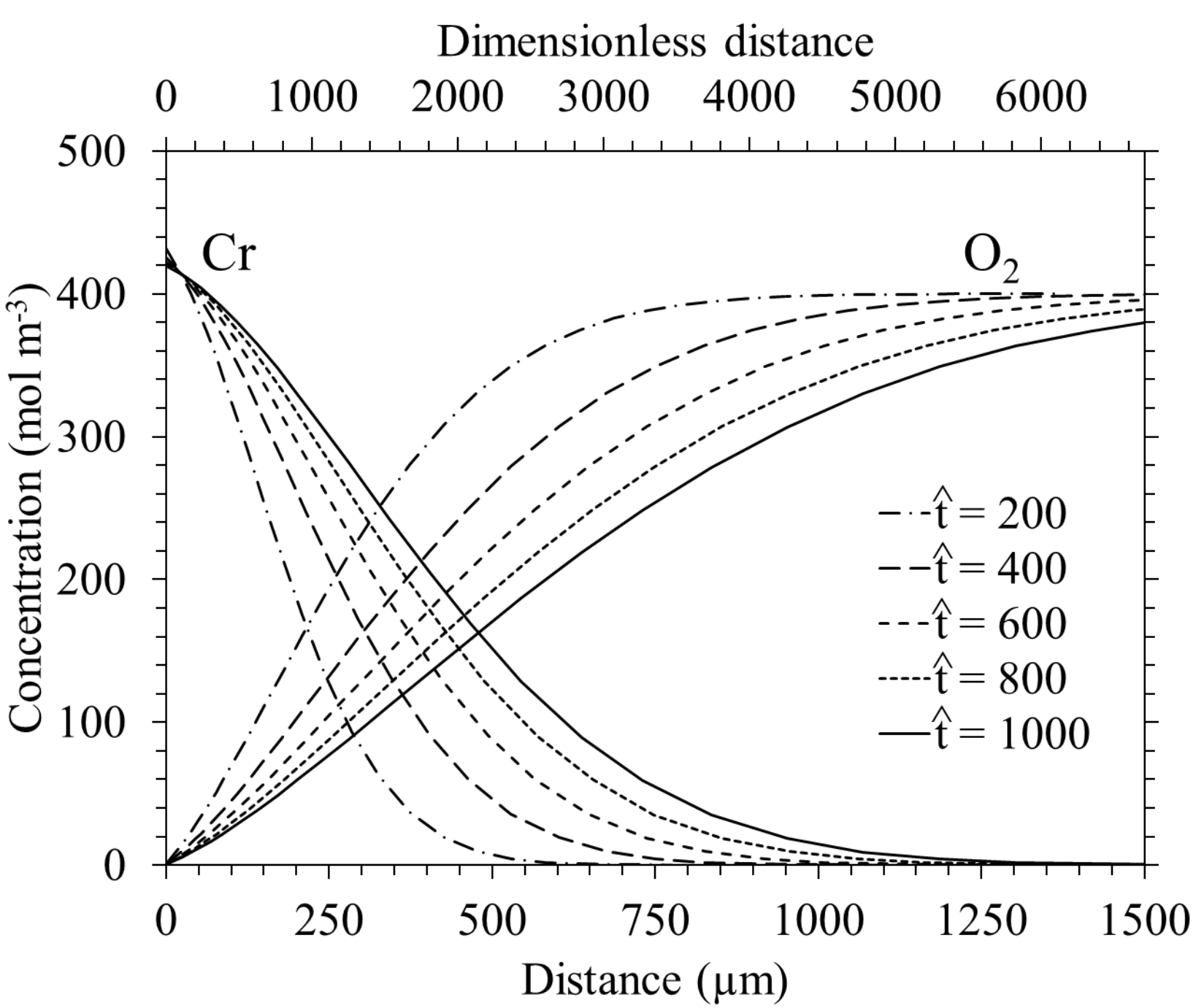
Dimensionless distance
0
1000
2000
3000
4000
5000
6000
500
400
300
200
100
0
Cr
O2
Concentration (mol m-3)
t̂ = 200
t̂ = 400
t̂ = 600
t̂ = 800
t̂ = 1000
0
250
500
750
1000
1250
1500
Distance (μm)

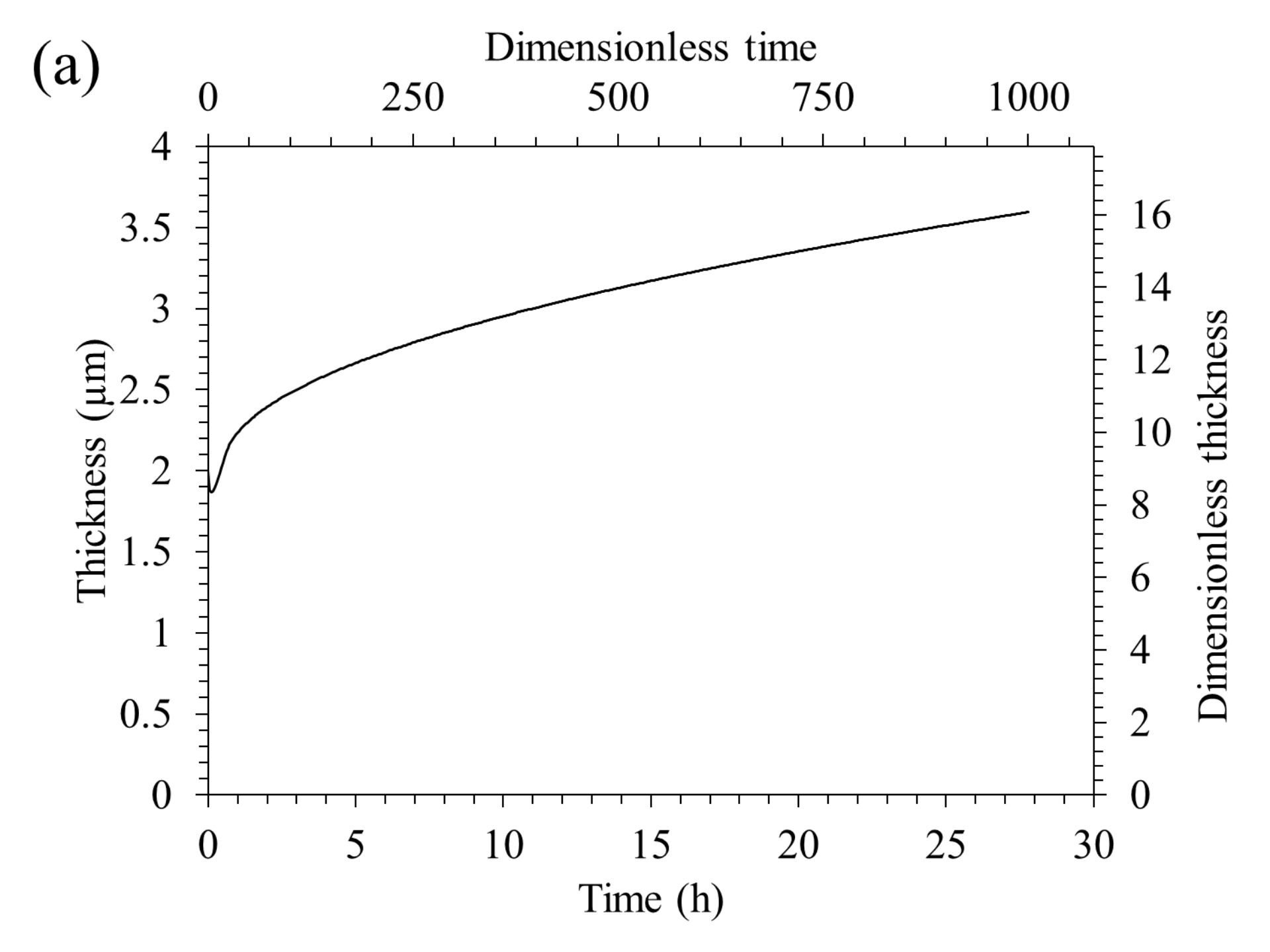
(a)
Dimensionless time
0
250
500
750
1000
Thickness (μm)
4
3.5
3
2.5
2
1.5
1
0.5
0
Dimensionless thickness
16
14
12
10
8
6
4
2
0
0
5
10
15
20
25
30
Time (h)

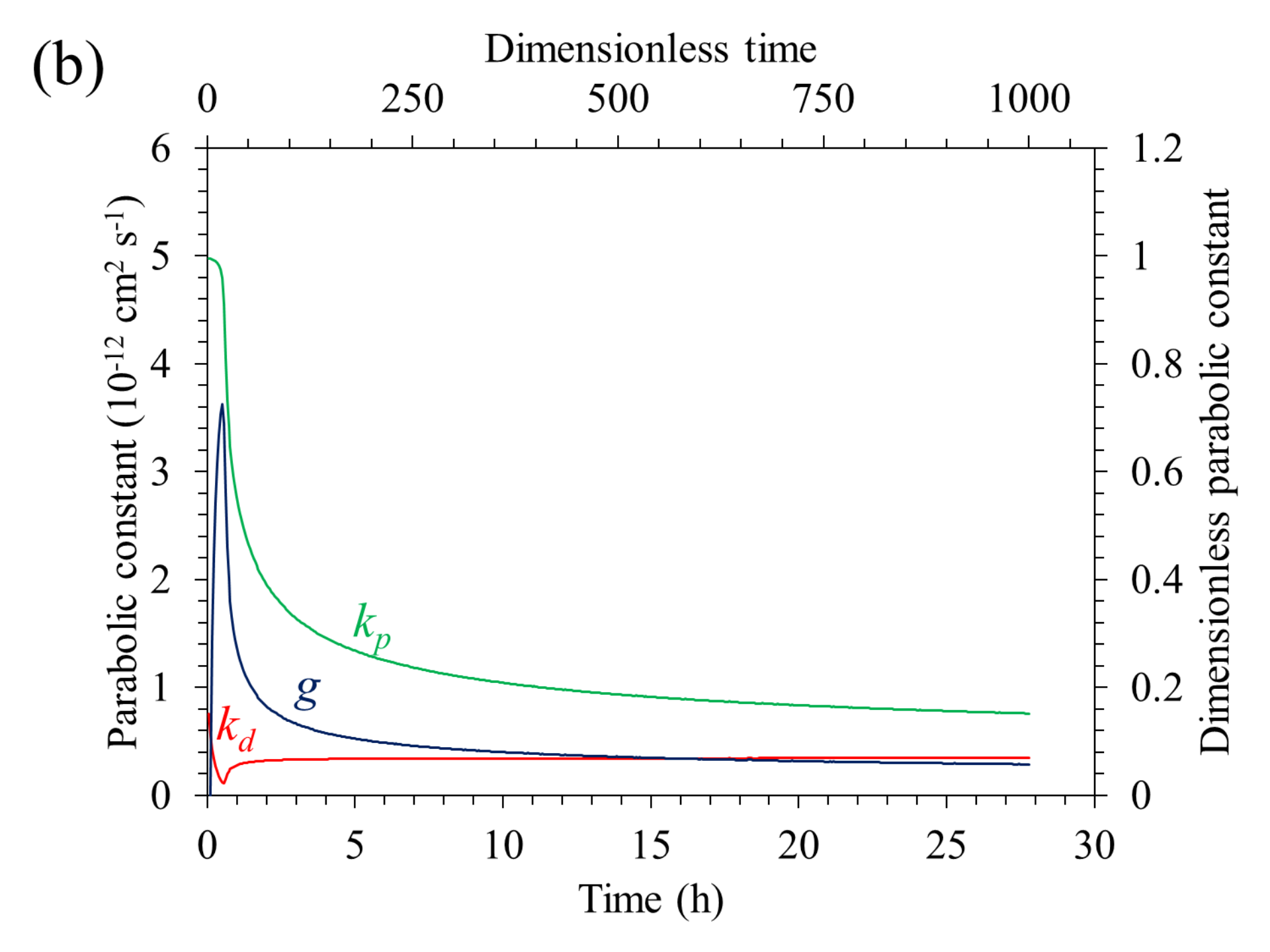
(b)
Dimensionless time
0
250
500
750
1000
Parabolic constant (10^{-12} cm^2 s^{-1})
Dimensionless parabolic constant
0
1
2
3
4
5
6
0
0.2
0.4
0.6
0.8
1
1.2
k_p
g
k_d
0
5
10
15
20
25
30
Time (h)

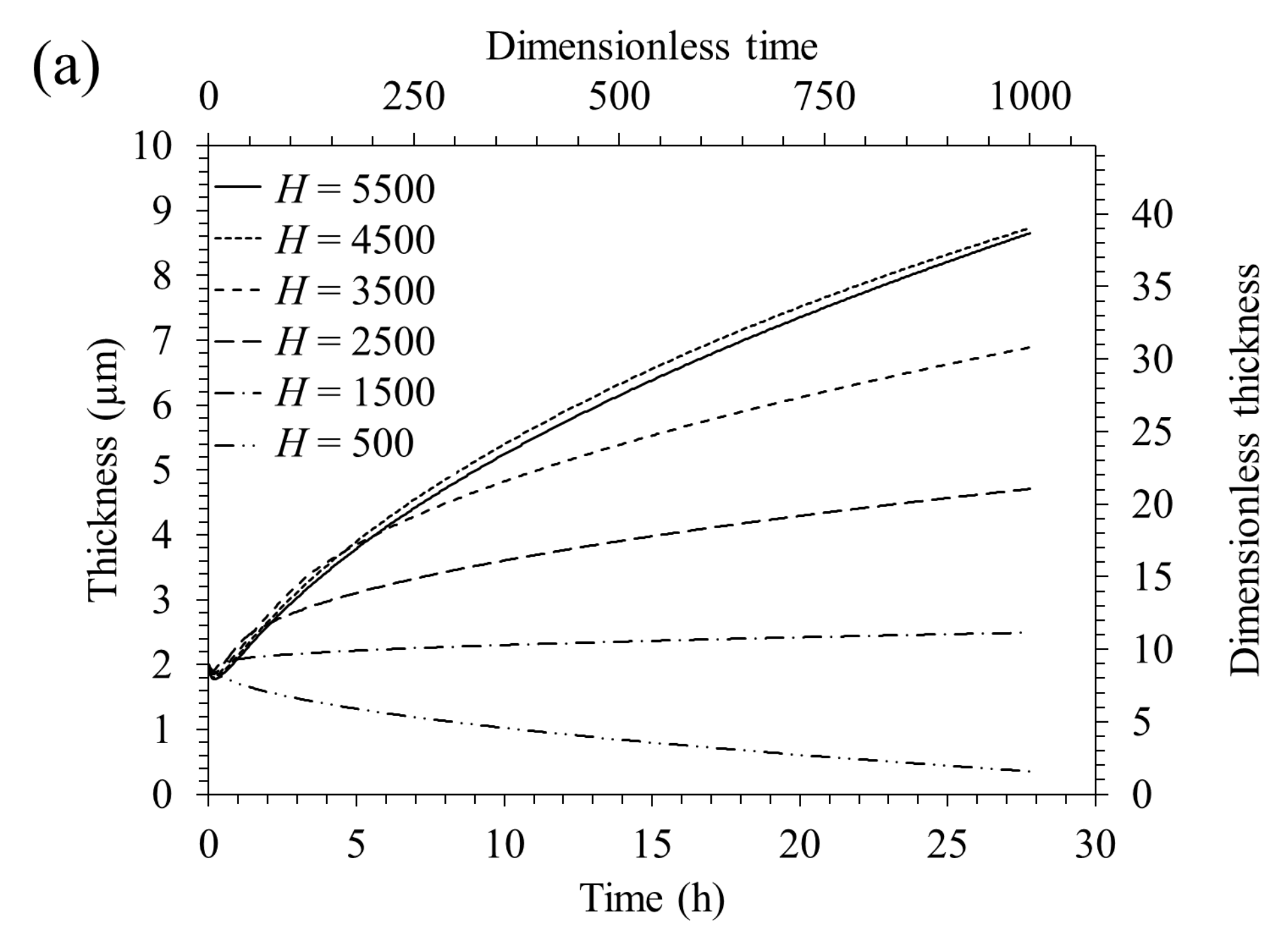
(a)
Dimensionless time
0
250
500
750
1000
10
9
8
7
6
5
4
3
2
1
0
H = 5500
H = 4500
H = 3500
H = 2500
H = 1500
H = 500
Thickness (μm)
40
35
30
25
20
15
10
5
0
Dimensionless thickness
0
5
10
15
20
25
30
Time (h)

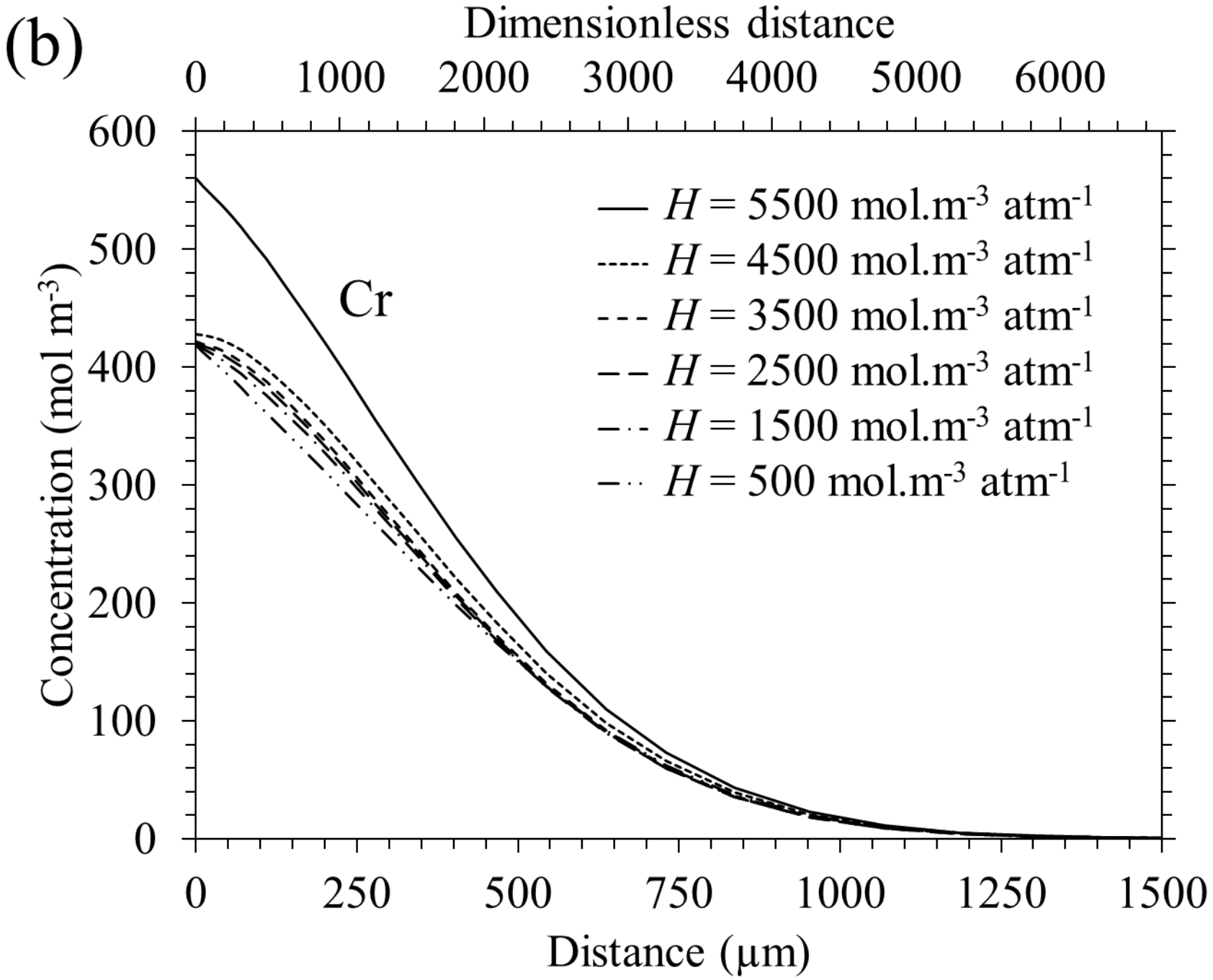
(b)
Dimensionless distance
0
1000
2000
3000
4000
5000
6000
600
500
400
300
200
100
0
Concentration (mol m-3)
Cr
H = 5500 mol.m-3 atm-1
H = 4500 mol.m-3 atm-1
H = 3500 mol.m-3 atm-1
H = 2500 mol.m-3 atm-1
H = 1500 mol.m-3 atm-1
H = 500 mol.m-3 atm-1
0
250
500
750
1000
1250
1500
Distance (μm)

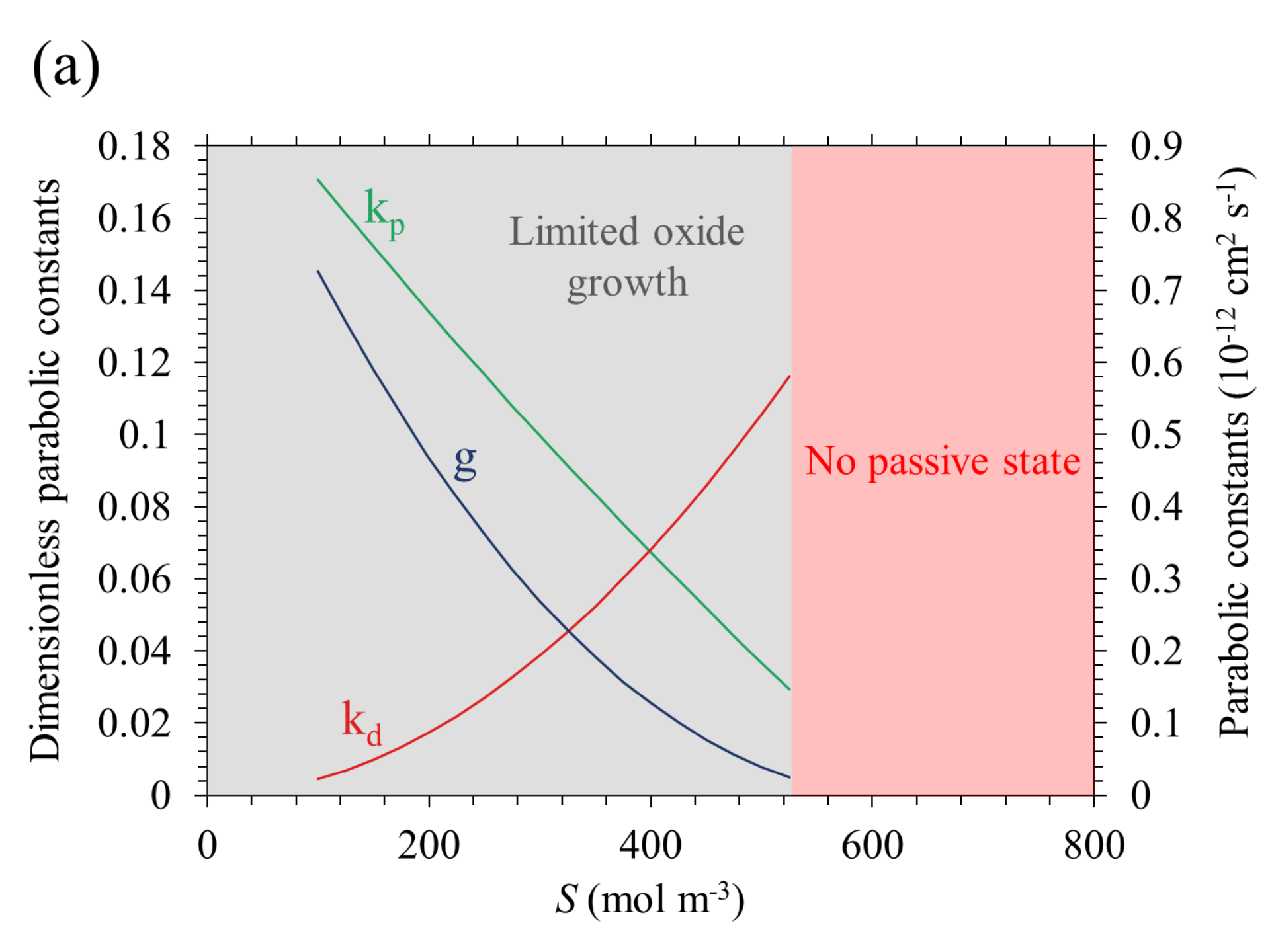
(a)
Limited oxide growth
No passive state
k_p
g
k_d
Dimensionless parabolic constants
Parabolic constants (10^{-12} cm^2 s^{-1})
S (mol m^{-3})
0
0.02
0.04
0.06
0.08
0.1
0.12
0.14
0.16
0.18
0.1
0.2
0.3
0.4
0.5
0.6
0.7
0.8
0.9
0
200
400
600
800

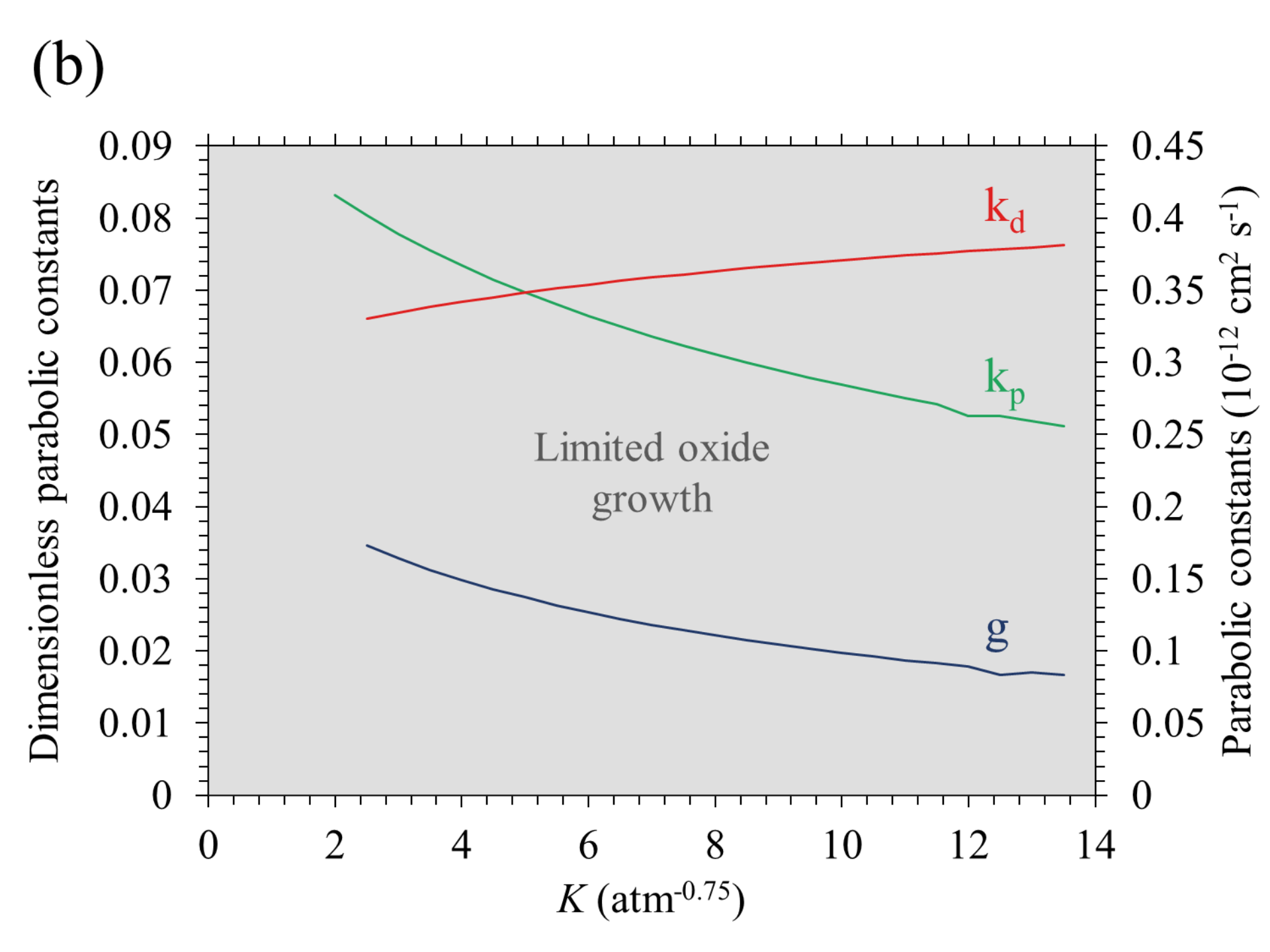
(b)
Dimensionless parabolic constants
Parabolic constants (10^{-12} cm^2 s^{-1})
K (atm$^{-0.75}$)
k_d
k_p
g
Limited oxide growth
0
0.01
0.02
0.03
0.04
0.05
0.06
0.07
0.08
0.09
0.05
0.1
0.15
0.2
0.25
0.3
0.35
0.4
0.45
0
2
4
6
8
10
12
14

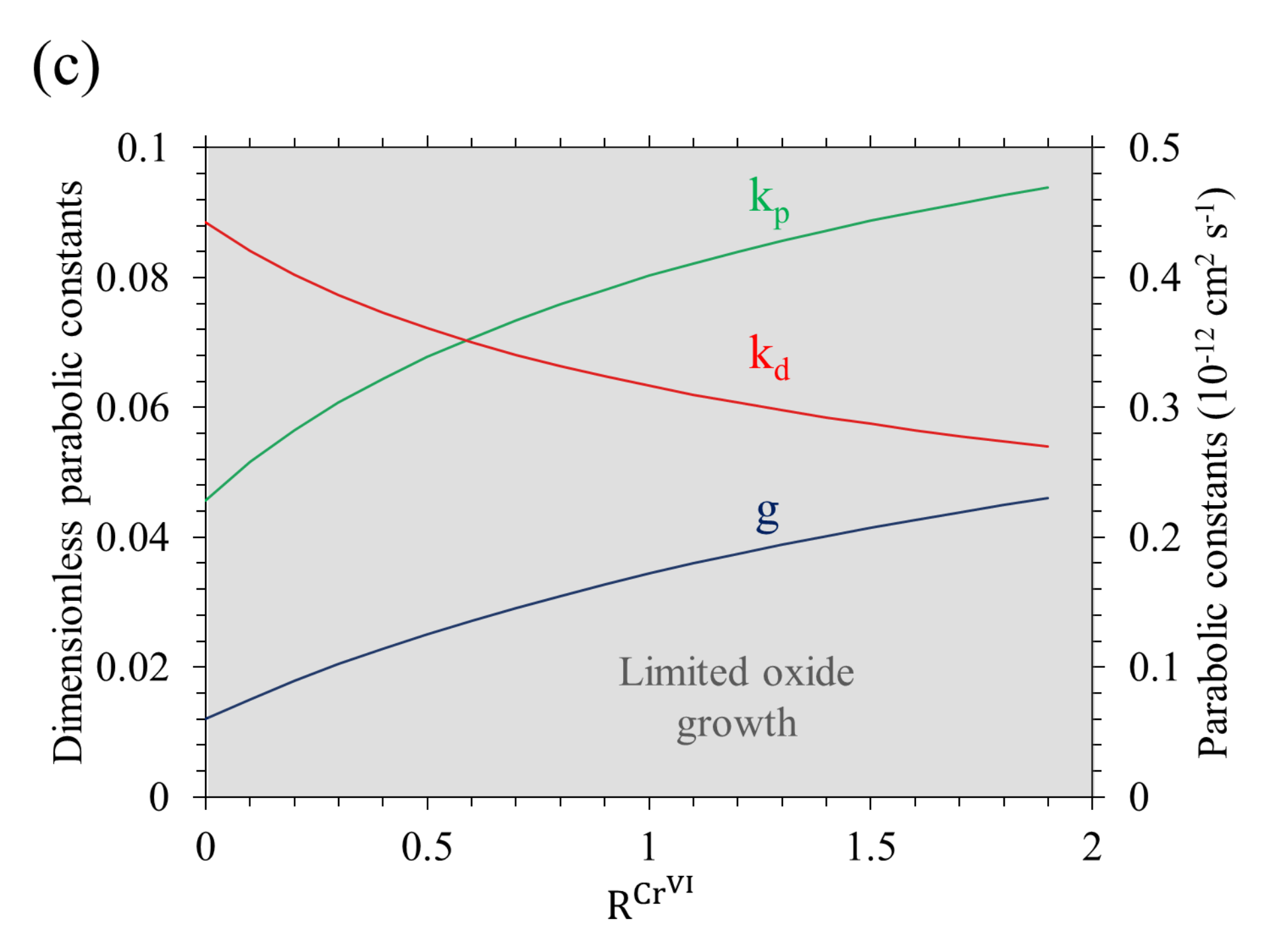
(c)
0.1
0.08
0.06
0.04
0.02
0
Dimensionless parabolic constants
0.5
0.4
0.3
0.2
0.1
0
Parabolic constants (10^{-12} cm^2 s^{-1})
k_p
k_d
g
Limited oxide growth
0
0.5
1
1.5
2
$R^{Cr^{VI}}$

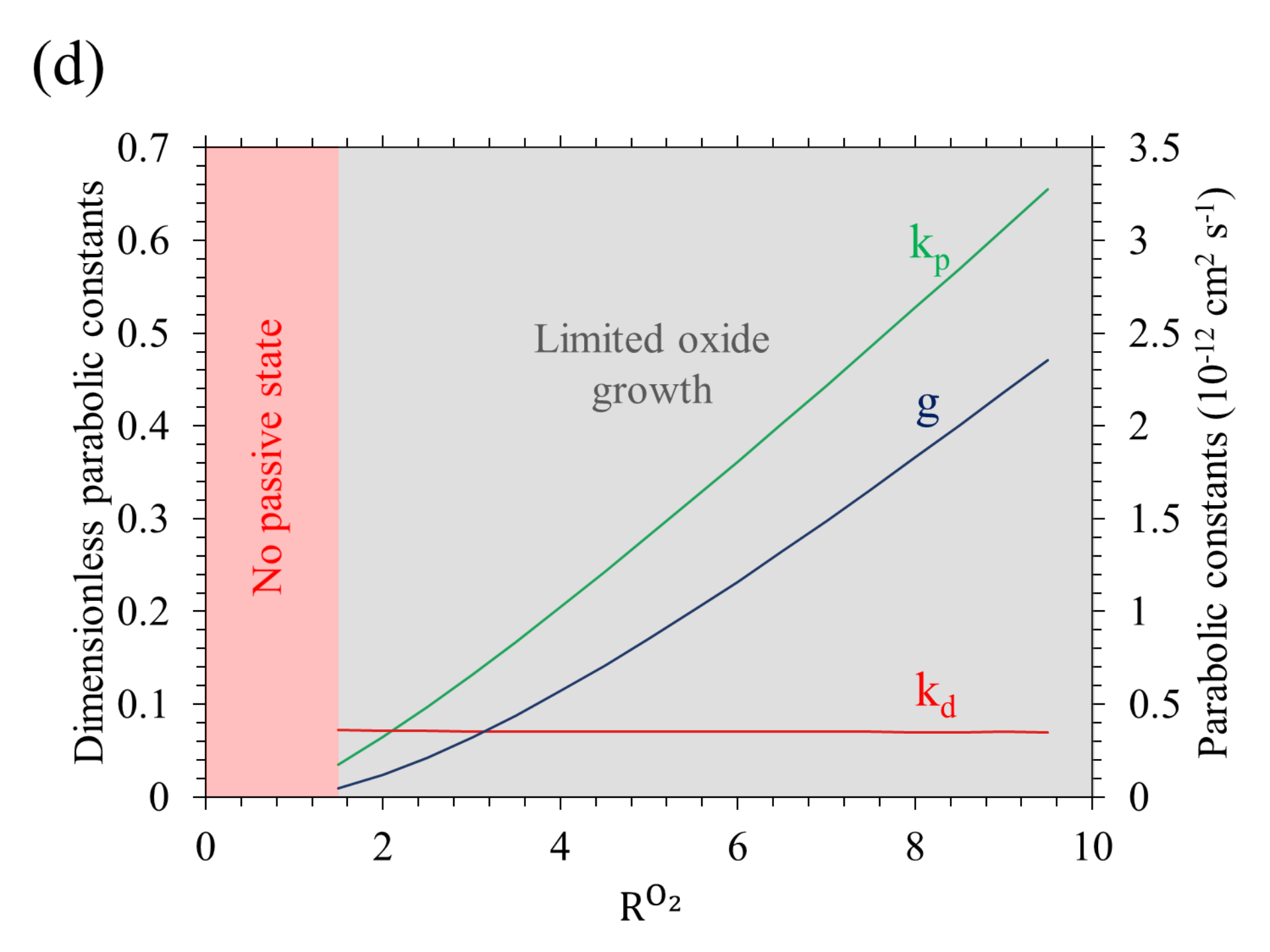
(d)
Dimensionless parabolic constants
Parabolic constants (10^{-12} cm^2 s^{-1})
R^{O_2}
No passive state
Limited oxide growth
k_p
g
k_d
0
0.1
0.2
0.3
0.4
0.5
0.6
0.7
0.5
1
1.5
2
2.5
3
3.5
0
2
4
6
8
10

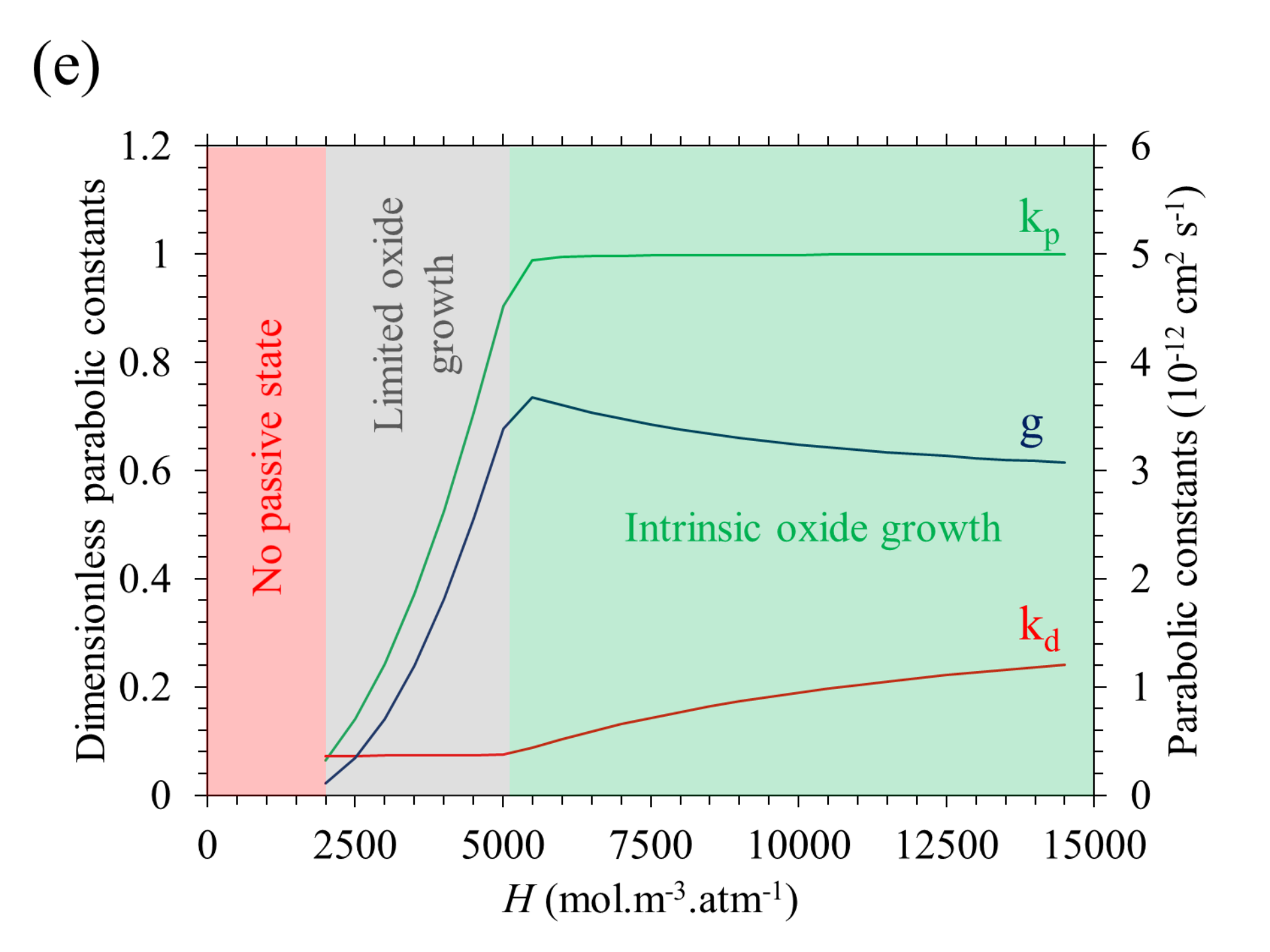
(e)
Dimensionless parabolic constants
Parabolic constants (10^{-12} cm^2 s^{-1})
H (mol.m^{-3}.atm^{-1})
No passive state
Limited oxide growth
Intrinsic oxide growth
k_p
g
k_d
0
0.2
0.4
0.6
0.8
1
1.2
0
1
2
3
4
5
6
0
2500
5000
7500
10000
12500
15000

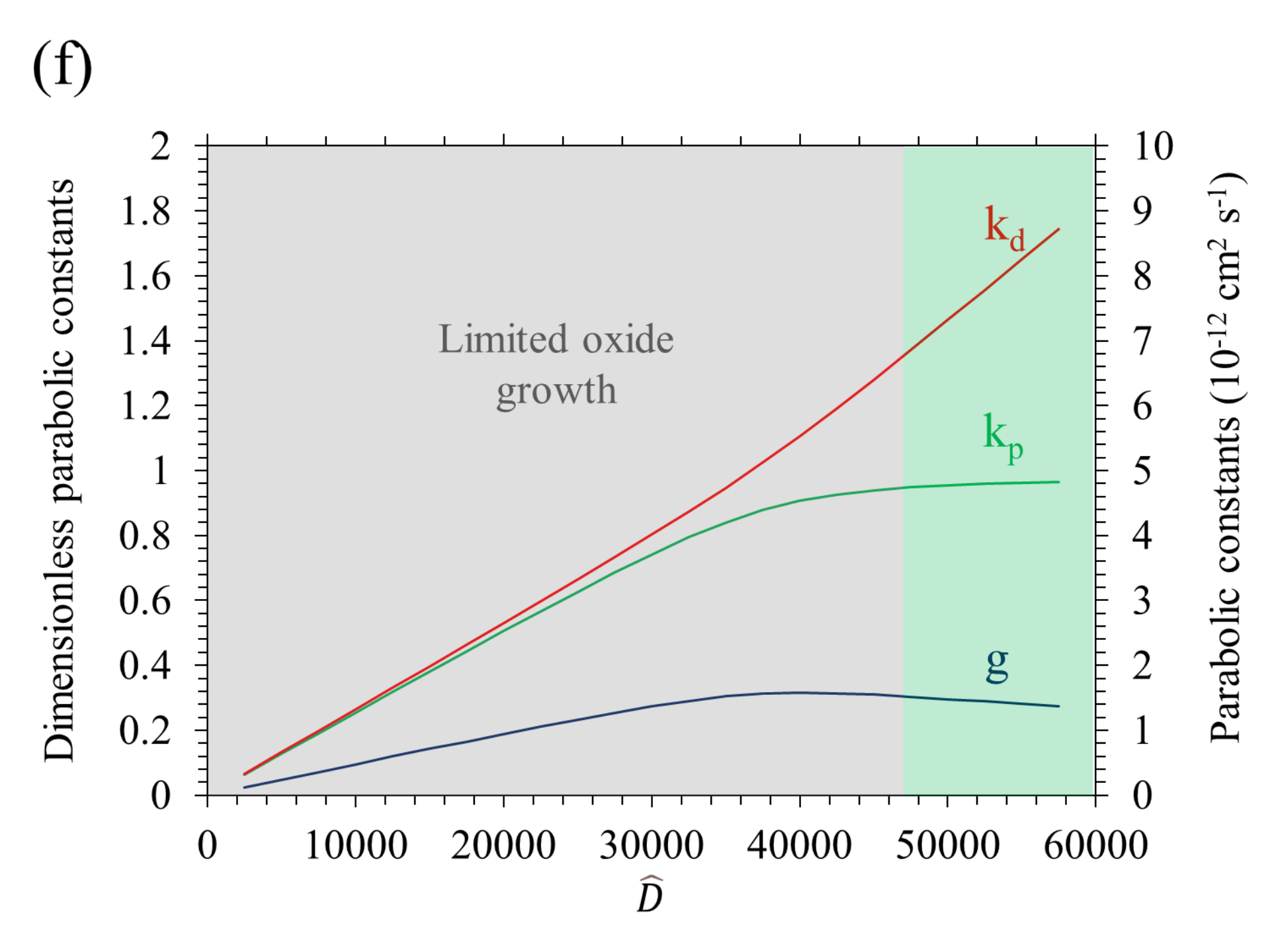
(f)
Dimensionless parabolic constants
Parabolic constants (10^{-12} cm^2 s^{-1})
Limited oxide growth
k_d
k_p
g
$\widehat{D}$
0
0.2
0.4
0.6
0.8
1
1.2
1.4
1.6
1.8
2
0
1
2
3
4
5
6
7
8
9
10
0
10000
20000
30000
40000
50000
60000

Identification of the relevant corrosion phenomena

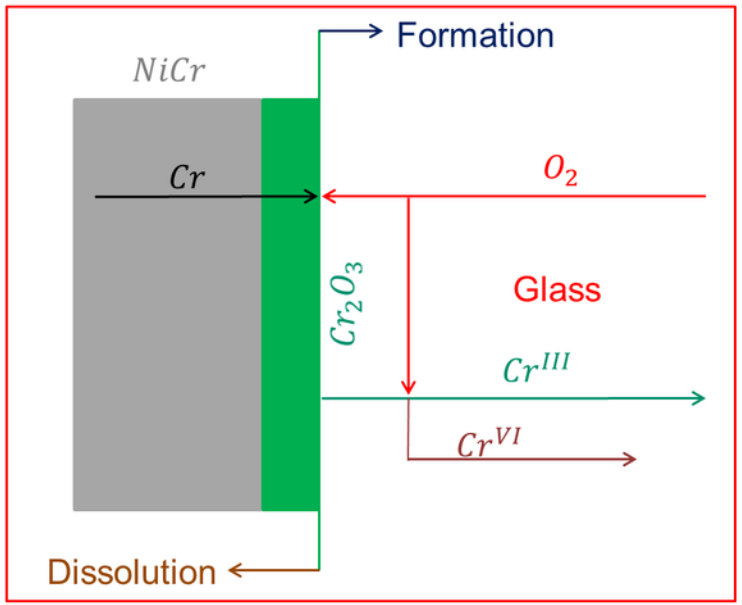

Identification of 6 parameters
S, K, H, $\widehat{D}$, $R^{Cr^{VI}}$ and R^{O_2}

Modeling and simulation

Evolution of the oxide thickness $e_{(t)}$

$$\frac{de}{dt} = Formation\ rate - Dissolution\ rate$$

$$\frac{k_p}{e} \qquad \sqrt{\frac{k_d}{2t}}$$

Protected alloy
$e_{(t)} = \sqrt{2gt}$

Depassivation
$e_{(t)} = 0$

Influences of the 6 parameters on the corrosion behavior of a chromia-forming alloy